



HAL
open science

Streaming Potential Coupling Coefficient and Transport Properties of Unsaturated Carbonate Rocks

Aurélien Cherubini, Bruno Garcia, Adrian Cerepi, André Revil

► **To cite this version:**

Aurélien Cherubini, Bruno Garcia, Adrian Cerepi, André Revil. Streaming Potential Coupling Coefficient and Transport Properties of Unsaturated Carbonate Rocks. *Vadose Zone Journal*, 2018, 17 (1), pp.1-12. 10.2136/vzj2018.02.0030 . hal-01941002

HAL Id: hal-01941002

<https://ifp.hal.science/hal-01941002>

Submitted on 30 Nov 2018

HAL is a multi-disciplinary open access archive for the deposit and dissemination of scientific research documents, whether they are published or not. The documents may come from teaching and research institutions in France or abroad, or from public or private research centers.

L'archive ouverte pluridisciplinaire **HAL**, est destinée au dépôt et à la diffusion de documents scientifiques de niveau recherche, publiés ou non, émanant des établissements d'enseignement et de recherche français ou étrangers, des laboratoires publics ou privés.



Distributed under a Creative Commons Attribution - NonCommercial - NoDerivatives 4.0 International License

Original Research

Core Ideas

- Streaming potential coupling coefficient is dependent on saturation in carbonate rocks.
- Salinity influences the streaming potential coupling coefficient.
- Water relative permeability can be estimated from streaming potential measurements.
- Transport properties of carbonate rocks can be modeled using the van Genuchten approach.

A. Cherubini and B. Garcia, GeoFluids and Rocks Dep., IFP Energies Nouvelles—Geosciences Division, 92852 Rueil-Malmaison, France; A. Cherubini and A. Cerepi, EA 4592 Géoressources et Environnement, ENSEGD-Bordeaux INP, 33607 Pessac, France; A. Revil, Univ. Grenoble Alpes, Univ. Savoie Mont Blanc, CNRS, IRD, IFTTAR, ISTerre, 38000 Grenoble, France. *Corresponding author (aurelien.cherubini@ifpen.fr).

Received 6 Feb. 2018.

Accepted 11 July 2018.

Citation: Cherubini, A., B. Garcia, A. Cerepi, and A. Revil. 2018. Streaming potential coupling coefficient and transport properties of unsaturated carbonate rocks. *Vadose Zone J.* 17:180030. doi:10.2136/vzj2018.02.0030

© Soil Science Society of America. This is an open access article distributed under the CC BY-NC-ND license (<http://creativecommons.org/licenses/by-nc-nd/4.0/>).

Streaming Potential Coupling Coefficient and Transport Properties of Unsaturated Carbonate Rocks

A. Cherubini,* B. Garcia, A. Cerepi, and A. Revil

We measured the streaming potential coupling coefficient of natural saturated and unsaturated carbonate rocks. Saturation was achieved with NaCl brines with salinities ranging from 2×10^{-3} to 2.0 mol L^{-1} . The magnitude of the coupling coefficient increased with decreasing salinity, similarly to the trend observed for sandstones. The permeability had a low impact on the values of the streaming potential coupling coefficient at high and low salinity. The zeta potential was calculated at full saturation using a modified version of the Helmholtz–Smoluchowski equation that accounts for surface electrical conductivity. Under atmospheric conditions, the magnitude of the zeta potential decreased with the increase in salinity. We also explored the relationships between the streaming potential coupling coefficient and water saturation in three partially saturated limestones using a steady-state flow experiment. We found good agreement between the van Genuchten approach and experimental data, and fitted both the relative permeability and capillary pressure curves with the same value of the van Genuchten exponent m_v . We validated the predictive water relative permeability model described by Revil in water-wet rocks when the second fluid phase is non-polar.

Self-potential monitoring is a passive geophysical method based on the measurement of natural electrical fields in the subsurface of the Earth and provides data that are sensitive to water flow (Thony et al., 1997). Among the different processes involved in the variation of these electric fields, electrokinetic processes often tend to dominate in the vadose zone. They have already been studied in unsaturated clayey (Jougnot et al., 2012) or sandy (Mboh et al., 2012) soils and dolomites (Revil and Cerepi, 2004; Revil et al., 2007), but there exist few experiments in unsaturated intact limestones (Cerepi et al., 2017). Streaming potential signals are due to the presence of an electrical double layer at the charged interface of the grains in porous media (Stern, 1924; Overbeek, 1952; Dukhin and Derjaguin, 1974).

The water–calcite interface has been increasingly studied in the last decade due to its use in a large range of applications including CO_2 sequestration (Kaszuba et al., 2003; Xu et al., 2003; Lerouge et al., 2010) and oil extraction from carbonate reservoirs (Zullig and Morse, 1988). Complexation models can be used in concert with electrical double layer theory to compute the electrochemical properties of the water–calcite interface (Wolthers et al., 2008, 2012). Recently, Li et al. (2016) focused their work on the surface conductivity effects on the zeta potential of calcite. They showed that the classical Helmholtz–Smoluchowski equation underestimates the zeta potential of calcite at low salinities and that surface conductivity should be included in the expression of the streaming potential coupling coefficient. This coefficient relates the fluid and streaming potential gradients when the total current density is zero (e.g., Sill, 1983). In unsaturated porous media, Revil et al. (1999b) established a relationship between the texture of porous media and this coefficient, later exploited by different researchers (Revil et al., 2007; Jougnot et al., 2012; Cerepi et al., 2017).

Our goal in this study was to provide new experimental evidence for the dependence of the streaming potential coupling coefficient of carbonate rocks with the saturation, comparing our data with the predictive model developed by Revil et al. (2007), including

the Corey or the van Genuchten exponent, often used to describe multiphase flow in the vadose zone. The water relative permeability has been calculated and successfully compared with the prediction of the model given by Revil et al. (2007). Mboh et al. (2012) showed that the capillary pressure curves, the relative permeability, and the relative streaming potential coefficient could be described in a consistent way for a silica sand.

A new core flooding system based on the study of Cerepi et al. (2017) allowed us to provide the first experiments to date that could measure simultaneously the relative permeability and the streaming potential coupling coefficient for unsaturated carbonates. We show that the relative permeability, the relative streaming potential coupling coefficient, and the capillary pressure can be described in a consistent way for carbonates using the van Genuchten approach.

Theory

Streaming Potential Coupling Coefficient

Revil and Mahardika (2013) defined the generalized cross-coupled $L(\omega)$ (of electrokinetic nature) Ohm and Darcy constitutive laws for the Darcy velocity \mathbf{w}_w (m), which is the filtration displacement of the fluid with respect to the solid, and the electrical current density \mathbf{J} (A m^{-2}) under unsaturated conditions:

$$\begin{bmatrix} \mathbf{J} \\ \mathbf{w}_w \end{bmatrix} = \begin{bmatrix} \sigma(S_w) & L(S_w) \\ L(S_w) & \frac{k(S_w)}{\eta_w} \end{bmatrix} \begin{bmatrix} \mathbf{E} \\ -\nabla p \end{bmatrix} \quad [1]$$

$$L(\omega) = \frac{k(S_w) \hat{Q}_v(S_w)}{\eta_w} \quad [2]$$

where $\sigma(S_w)$ (S m^{-1}) is the electrical conductivity, $k(S_w)$ (m^2) is the permeability, \hat{Q}_v (C m^{-3}) is the dynamic excess of charge dragged by the electrolyte (given by a volume average of the local current density given by the local charge density of the diffuse layer times the local fluid flow velocity), η_w (Pa s) is the dynamic viscosity of the water phase, \mathbf{E} (V m^{-1}) is the electrical field, p (Pa) is the pore fluid pressure, and S_w (dimensionless) is the water saturation. The streaming potential coupling coefficient is given by (Linde et al., 2007; Revil et al., 2007)

$$C(S_w) = \left(\frac{\partial \varphi}{\partial p} \right)_{\mathbf{J}=0} \quad [3]$$

$$C(S_w) = - \frac{L(S_w)}{\sigma(S_w)} \quad [4]$$

$$C(S_w) = - \frac{k(S_w) \hat{Q}_v(S_w)}{\eta_w \sigma(S_w)} \quad [5]$$

where φ is the electrostatic potential of electrokinetic nature. According to Revil and Mahardika (2013), the permeability and effective charge density depend on saturation:

$$k(S_w) = k_r(S_w) k_0 \quad [6]$$

$$\hat{Q}_v(S_w) = \frac{\hat{Q}_v^0}{S_w} \quad [7]$$

where \hat{Q}_v^0 and k_0 are the effective charge density and the permeability at saturation, respectively.

Saturation Dependence of the Streaming Potential Coupling Coefficient

The resistivity index I_r is defined thanks to the classical second Archie's law (Archie, 1942), for high ionic strengths ($\geq 0.1 \text{ mol L}^{-1}$), when grain surface conductivity can be neglected compared with bulk water conductivity, as

$$I_r \equiv \frac{\sigma_w}{\sigma(S_w) F} = S_w^{-n} \quad [8]$$

where F is the formation factor and n is the second Archie's exponent.

One of the most popular models to describe the influence of saturation on the relative permeability is the Brooks and Corey (1964, 1966) model. The Brooks and Corey relationships for the relative wetting and non-wetting fluid permeabilities are

$$k_{rw} = S_c^{N_w} \quad [9]$$

$$k_{rg} = (1 - S_c)^2 (1 - S_c^{N_g}) \quad [10]$$

with

$$S_c = \left(\frac{S_w - S_{wi}}{1 - S_{wi}} \right) \quad [11]$$

where S_{wi} and S_c are the irreducible water saturation and the effective water saturation, respectively, and N_w and N_g are the Corey exponents for the water and gas phases, respectively. Alternatively, the water relative permeability can be explained from the equation of van Genuchten (1980) with the fitting parameter m_v :

$$k_{rw} = \sqrt{S_c} \left[1 - (1 - S_c^{1/m_v})^{m_v} \right]^2 \quad [12]$$

The index m_v can also be derived from the capillary pressure curve (van Genuchten, 1980) as

$$P_c = P_c (S_c^{-1/m_v} - 1)^{1-m_v} \quad [13]$$

where P_c and P_{c_e} denote the capillary pressure and the capillary entry pressure of water in the rock, respectively.

Revil et al. (2007) proposed a relationship from modeling (also tested by Cerepi et al. [2017] in an experimental approach) between the relative permeability and the saturation using the streaming potential coupling coefficient, Archie's exponent, and the water Corey exponent from Brooks and Corey (1964) as

$$k_r(S_w) = S_w^{n+1} C_r(S_w) \quad [14]$$

with a relative streaming potential coupling coefficient (ratio of the coupling coefficient at saturation S_w to the value of the coupling coefficient at saturation) given by

$$C_r(S_w) = \frac{C(S_w)}{C_{\text{sat}}} = \frac{1}{S_w^{n+1}} \left(\frac{S_w - S_{wi}}{1 - S_{wi}} \right)^{N_w} \quad [15]$$

Alternatively, using the van Genuchten exponent, we have

$$C_r(S_w) = S_w^{-(n+1)} \sqrt{S_c} \left[1 - \left(1 - S_c^{1/m_v} \right)^{m_v} \right]^2 \quad [16]$$

Zeta Potential

Under steady-state conditions, the zeta potential is calculated from the streaming potential coefficient using the well-known Helmholtz–Smoluchowski equation in the absence of surface conduction in the electrical double layer (e.g., Hunter, 1981):

$$C_{\text{sat}} = \frac{\varepsilon_w \zeta}{\eta_w \sigma_w} \quad [17]$$

where ε (F m^{-1}) is the dielectric permittivity, ζ (V) is the zeta potential, and σ_w (S m^{-1}) is the electrical conductivity of the brine saturating the rock. When the surface conductivity is non-negligible (e.g., Revil et al., 1999a; Guichet et al., 2006; Alroudhan et al., 2016; Li et al., 2016), the zeta potential is related to the streaming potential coupling coefficient using the formation factor, F , which is the ratio of the conductivity of the electrolyte to the conductivity of the saturated rock sample when surface conductivity is

negligible, and the electrical conductivity of the saturated porous material, $\sigma(S_w = 1)$:

$$C_{\text{sat}} = \frac{\varepsilon_w \zeta}{\eta_w \sigma(S_w = 1) F} \quad [18]$$

At low salinity, the evolution of the zeta potential was predicted by theoretical models, based on the Nernst–Planck–Poisson–Boltzmann transport equation (Revil et al., 1999a). Pride and Morgan (1991) found a logarithmic relationship in silica materials that relates the zeta potential with brine salinity, and Jaafar et al. (2009) suggested that the zeta potential is constant at high salinity ($>0.4 \text{ mol L}^{-1}$) also in silica-based materials:

$$\zeta = a + b \log_{10} C_f, \quad C_f < 0.4 \text{ mol L} \quad [19]$$

$$\zeta = c, \quad C_f \geq 0.4 \text{ mol L}^{-1} \quad [20]$$

where a , b , and c are constant values and C_f is the brine salinity (mol L^{-1}).

Experimental Methodology

Apparatus

The experimental setup used to measure the streaming potential coupling coefficient, the electrical conductivity, and the permeability under unsaturated conditions is shown in Fig. 1. The experiments are performed on cylindrical limestone core samples, wrapped in a rubber sleeve and confined within a core holder with

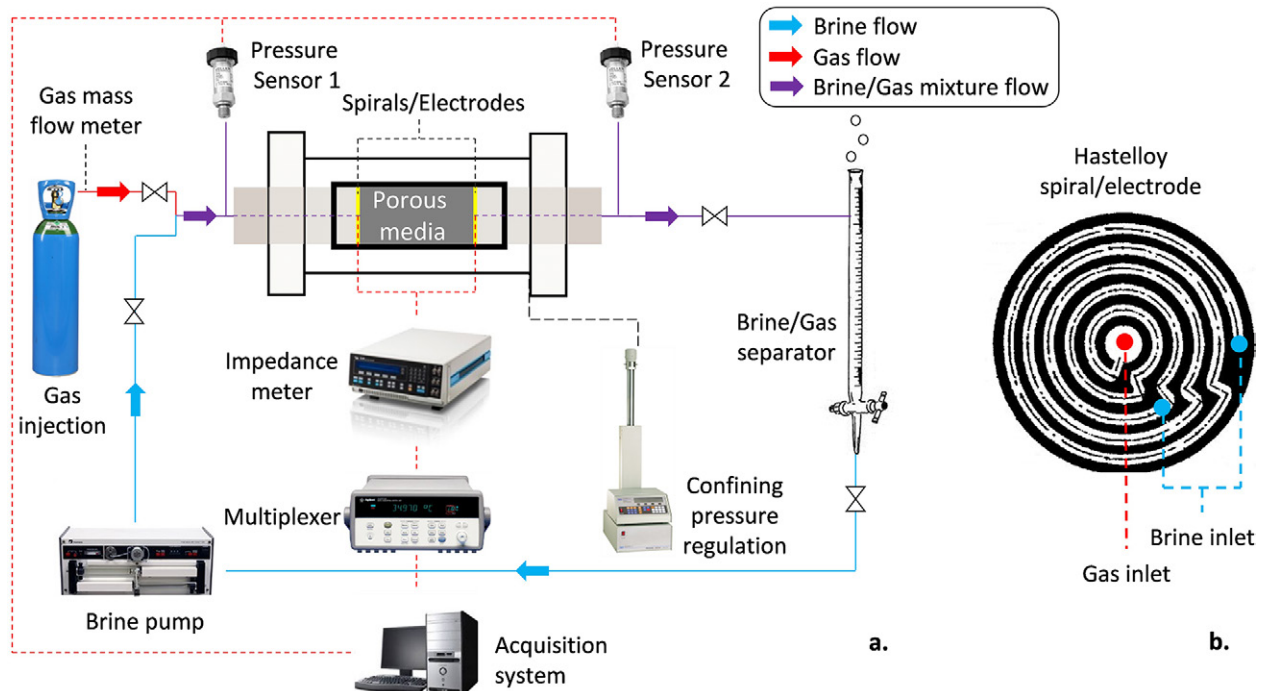


Fig. 1. Experimental apparatus for measuring the relative permeability and the streaming potential coupling coefficient: (a) simplified sketch of the apparatus with fluid flow lines (solid lines) and electrical connections (dashed lines); and (b) sketch of the non-polarizable Hastelloy electrode used to measure the streaming potential coupling coefficient and the sample resistivity with a frequency equals to 1 kHz. Note that the electrode has the same diameter as the sample wrapped in the sleeve and allows injection of gas and brine simultaneously in the sample.

a confining pressure of 3×10^6 Pa. This pressure is regulated by a pump to avoid temperature variations of the room and was constant throughout the experiment. Experiments were controlled with X-ray imaging to verify that there was no brine flowing along the external face of the sample and the rubber sleeve. The stainless steel body of the core holder does not come into contact with the sample or fluids and is electrically connected to the Earth.

The electrical and relative permeability experimental measurements were performed using a steady-state flooding system, allowing us to inject brine and gas simultaneously into the sample (rocks are water wet). One pump was used to inject brine into the core at a constant flow rate, while a gas flow regulator (Bonkorst F-201-CV) regulated the flow of gas (only N_2 was used in this study to avoid any chemical reaction with carbonates and gas). The brine used for electrical measurements during the multiphase flow experiments was comprised of only 10 g L^{-1} (0.17 mol L^{-1}) NaCl in deionized water and had a conductivity of 1.58 S m^{-1} . A separator allows separation of the brine and gas at the outlet of the sample by gravity. The gas goes into the atmosphere while the brine is pumped again by the pump. The brine saturation decreases, whereas the gas saturation increases until the irreducible water saturation. The brine/gas flow rate ratio decreases during the drainage phase. The pressure difference measured for each brine/gas ratio permits measurement of the relative permeabilities using Darcy's law when steady state is reached and the water saturation in the sample no longer varies. For each saturation step, the electrical conductivity of the sample (at a frequency of 1 kHz) and the streaming potential coupling coefficient are measured. The stabilization process between brine and gas in the sample is extremely fast and controlled by a scanner. This process allows calculation of the irreducible water saturation with an accuracy of 1% and avoids measurement saturation errors due to the drying of the porous medium after the passage of the gas. At the same time, the capillary curves of the samples are investigated with a porous plate apparatus.

This setup gave us the possibility to measure the streaming potential coupling coefficient under saturated and unsaturated conditions thanks to two non-polarizable Hastelloy (superalloy nickel-based, highly resistant to corrosion) circular electrodes placed on the cross-section of the sample. These electrodes have strictly the same diameter as the samples. The non-polarizable electrodes present a spiral shape and allow injection of the gas at the center of the sample cross-section and the brine at two other positions in order not to create preferential paths. The gas migration and the saturation were controlled with a scanner in real time.

Core Samples

Nine carbonate core samples (Table 1) were investigated in this study at full brine saturation and different brine concentrations: two algal rhodolith packstones (ESTA1 and ESTA2) from Provence (southeastern France), three ooid grainstones (BRAU1, BRAU2, and BRAU3) from Meuse (eastern France), two lithoclast packstones (RFF1 and RFF2), one asteries grainstone (STE1) from Saint-Emilion (southwestern France), and one wackestone (LAV1)

Table 1. Petrophysical characteristics of the limestone samples studied, including water porosity (φ_w), scanner porosity (φ_{scan}), absolute permeability (k_0), formation factor (F), Archie's saturation (n) exponent, Corey exponent for water (N_w), irreducible water saturation (S_{wi}), van Genuchten exponent (m_v), and entry pressure of water (P_c).

Sample	φ_w	φ_{scan}	k_0	F	n	N_w	S_{wi}	m_v	P_c
	— % —		mD	kPa					
BRAU1	30	30	80	24.0	2.0	—	—	—	—
BRAU2	25	—	7	24.5	2.5	9	0.30	0.54	16
BRAU3	30	29	80	22.1	2.0	—	—	—	—
ESTA1	25	27	59	17.1	2.5	—	—	—	—
ESTA2	28	—	160	16.4	1.9	8	0.31	0.52	12
LAV1	23	24	2	15.0	—	—	—	—	—
RFF1	33	34	26	13.1	2.3	—	—	—	—
RFF2	34	34	31	10.6	2.3	5	0.35	0.66	33
STE1	36	—	600	11.9	—	—	—	—	—

from Vienne (western France). Only three of them were investigated at partial brine saturation (BRAU2, ESTA2, and RFF2) during multiphase flow experiments at constant brine concentration (10 g L^{-1} NaCl).

All the core samples have a length of 80 mm and a cross-sectional diameter of 39 mm. They were drilled parallel to the stratification and dried in an oven (60°C) before each experiment. The petrophysical properties of each core sample, including water porosity (φ_w , calculated from the mass difference between saturated and dry samples), scanner porosity (φ_{scan} , calculated from computerized tomography), absolute permeability (k), formation factor (F), Archie's cementation (m) and saturation (n) exponents, the Corey exponents for water and gas (N_w and N_g), the van Genuchten exponent (m_v), irreducible water saturation (S_{wi}), and the entry pressure of water (P_c) are reported in the Table 1. The samples have been chosen based on their large range of permeability values ($0.002\text{--}0.6 \mu\text{m}^2$ or $2\text{--}600$ mD) with the aim to determine the influence of permeability on the electrokinetic properties of carbonate rocks.

Measurements of the Streaming Potential Coupling Coefficient

The streaming potential is created by injections of different brine flow rates in the sample, inducing a pressure and a potential difference between the inlet and the outlet of the sample (Fig. 2). The experiment for each sample at full saturation begins with an electrical potential reference measurement across the sample for a given fluid flow rate. The main parameter is the stability of the voltage between the inlet and the outlet of the sample. Then, another brine flow rate is applied, which induces instantaneous pressure and voltage differences across the sample. Data are recorded at a sampling frequency of 1 Hz. Different flow rates are induced to have a better accuracy in the calculation of the streaming potential coupling coefficient. The same process is

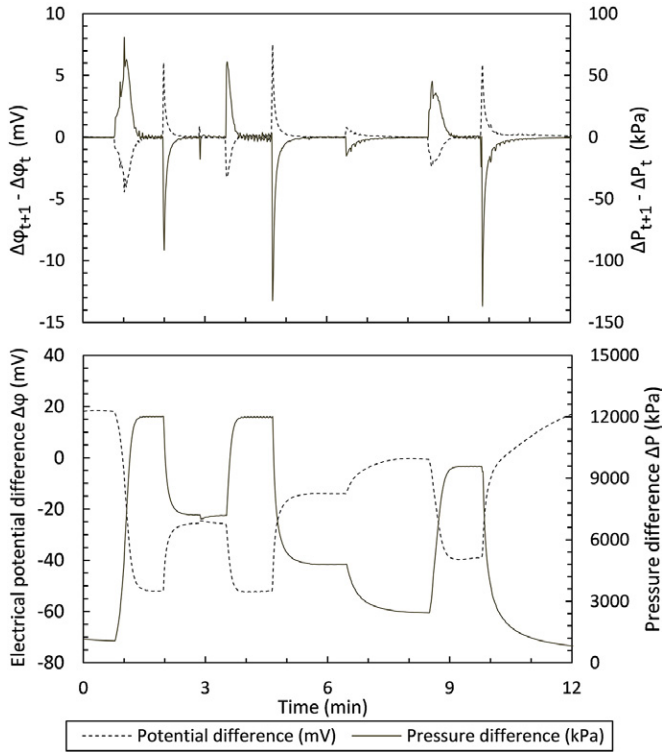


Fig. 2. Lavoux limestone (LAV1; permeability of $0.002 \mu\text{m}^2$) saturated with a NaCl brine at 1.0 g L^{-1} : (a) electrical potential and pressure difference along the core sample at $(t + 1) - t$ with a step measurement of 1 s (1 Hz)—the values are stabilized when they reach 0; an increase in the flow rate leads to an increase in the pressure difference and a decrease in the electrical potential difference between the inlet and the outlet of the core (note that all the peaks are in the opposite direction, which means that the streaming potential coupling coefficient has a negative value); and (b) an example of measured streaming potential vs. applied pressure difference for the same sample (LAV1) for a brine concentration of 1.0 g L^{-1} .

performed for each brine concentration. During the multiphase flow experiments, the streaming potential coupling coefficient is also measured at partial brine saturations. As mentioned above, the drainage phase of the sample is achieved by changing the flow rate ratio between brine and gas. The gas flow rate remains unchanged, while that of the water decreases. The streaming potential coupling coefficient is recorded when the brine flow rate is modified.

In the experiment, we did not impose backpressure (used to maintain constant pressure downstream) at the outlet of the sample. The outlet pressure remained equal to 100 kPa during all the experiments, under saturated and unsaturated conditions. To validate our protocol, we needed to test streaming potential measurements with different backpressures. The streaming potential coupling coefficient was measured on one sample (BRAU1) at a salinity of 10 g L^{-1} NaCl with three different backpressures of 100 kPa, 1 MPa, and 1.3 MPa (Fig. 3a). The value of the streaming potential coupling coefficient remained constant and was not affected by the backpressure. The same test was done for two other brine concentrations (30 and 40 g L^{-1} NaCl) with the same result (Fig. 3b). In conclusion, the streaming potential coupling

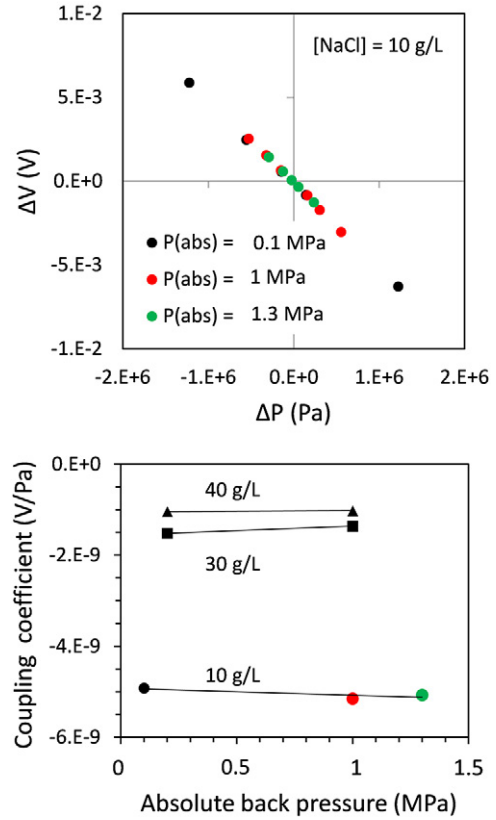


Fig. 3. Measurement of the streaming potential coupling coefficient for the BRAU1 sample: (a) measurements at 10 g L^{-1} NaCl and three different backpressures (100 kPa, 1 MPa, and 1.3 MPa); and (b) measurements of the streaming potential coupling coefficient at three brine concentrations (10, 30, and 40 g L^{-1}) and different backpressures.

coefficient is not affected by the backpressure whatever the brine NaCl concentration.

Measurements of Archie's Saturation Exponent

A two-electrode configuration was used to measure the conductivity of the brine-saturated and unsaturated sample. The electrical resistance of the system was measured at the frequency of 1 kHz between the two Hastelloy electrodes. The conductivity of the sample was calculated using

$$\sigma(S_w) = \frac{L}{R\pi r^2} \quad [21]$$

where R (Ω) is the sample resistance, L (m) is the length, and r (m) is the radius of the cylindrical core sample.

Calculation of the Zeta Potential

The zeta potential is calculated from the measured streaming potential coupling coefficient under fully saturated conditions using Eq. [18]. The formation factor (F) was calculated as the ratio of the resistivity of the sample filled with brine [$\sigma(S_w = 1)$] to the resistivity of the brine (σ_w), at high ionic strength (0.17 mol L^{-1}), when grain surface conductivity can be neglected compared with bulk conductivity:

$$F = \frac{\sigma_w}{\sigma(S_w = 1)} \quad [22]$$

The brine relative permittivity and the brine viscosity were adjusted as functions of temperature and salinity (e.g., Saunders et al., 2008). Measurements were performed under atmospheric conditions, without gas partial pressure.

Results

Relative Permeability

In Fig. 4a to 4c, we fit the relative permeability data calculated with a steady-state apparatus as a function of the saturation using the Brooks and Corey and the van Genuchten approaches for three samples: BRAU2, RFF2, and ESTA2. Corey exponents are equals to 9, 5, and 8, respectively, whereas van Genuchten exponents are 0.54, 0.66, and 0.52, respectively. The Corey exponents are in the same range as in previous studies that investigated relative permeabilities in a brine–gas system (Krevor et al., 2012). The van Genuchten exponents are also consistent because they are smaller than unity (Brooks and Corey, 1964).

Streaming Potential Coupling Coefficient

Effective Volumetric Charge Density Dependence

According to Jardani et al. (2007), recently discussed by Jougnot et al. (2015) and validated by a theoretical model (Guarracino and Jougnot, 2018), the volumetric charge density \hat{Q}_v^0 can be directly estimated from the quasi-static permeability in silica materials (at full saturation) by

$$\log_{10}(\hat{Q}_v^0) = -9.23 - 0.82 \log_{10}(k_0) \quad [23]$$

The samples studied have an absolute permeability in the range 0.002 to 0.6 μm^2 (Table 1) and streaming potential coupling coefficient values as reported in Table 2. Our values of volumetric charge densities for carbonates are slightly below the predictions of Eq. [23] (Fig. 5) and give an empirical law in the 0.002- to 0.6- μm^2 permeability range:

$$\log_{10}(\hat{Q}_v^0) = -11.37 - 0.94 \log_{10}(k_0) \quad [24]$$

In Fig. 6, data for five samples are represented depending on the salinity of the electrolyte, and compared with the theoretical value calculated from the model of Guarracino and Jougnot (2018). The excess charge density was calculated using the empirical zeta potential law that we define in this study (see Eq. [26] below) and the tortuosity formula from Winsauer et al. (1952). This model has never been applied to carbonates, but our data are consistent with other values calculated on limestone samples (Pengra et al., 1999; Revil et al., 2007).

Permeability Dependence

The streaming potential coupling coefficient was measured on different carbonate rock samples for three different NaCl concentrations (0.4, 1.0, and 10.0 g L^{-1}). The goal was to determine which

parameter between absolute permeability and brine concentration mainly controls the magnitude of the streaming potential coupling coefficient in carbonate rocks (Fig. 7). The streaming potential coupling coefficient seems independent of the permeability at saturation whatever the brine concentration (with a factor of 3 between low and high permeabilities). That said, its magnitude depends significantly on the brine concentration (factor of ~ 3000 between the measurements at 0.4 and 10 g L^{-1} NaCl). The brine concentration has therefore a much stronger influence on the magnitude of the streaming potential coupling coefficient than the permeability at saturation (Fig. 7).

Salinity Dependence

We establish now a relationship between the salinity of the NaCl electrolyte and the streaming potential coupling coefficient in the carbonate rocks. The streaming potential coupling coefficients were measured for the salinity range 0.002 to 2 mol L^{-1} . Nine samples were investigated for different brine concentrations (Fig. 8). The magnitude of the measured coupling coefficient decreased with increasing salinity. The trend between the magnitude of the streaming potential coupling coefficient and the salinity C_f (mol L^{-1}) is a power law ($R^2 = 0.96$):

$$C = -1.41 \times 10^{-9} C_f^{-0.862} \quad [25]$$

Vinogradov et al. (2010) also established an empirical relationship between the streaming potential coupling coefficient and brine salinity in sandstones and found a trend close to Eq. [24] (dashed line in Fig. 8).

Saturation Dependence

Measurements of the streaming potential coupling coefficient during the drainage phase of the samples by N_2 were made on three limestone cores: BRAU2, RFF2, and ESTA2. The relative streaming potential coupling coefficient is determined from the ratio between its value under unsaturated and saturated conditions (Fig. 4d–4i). The three samples exhibit a non-monotonic decrease of the relative streaming potential coupling coefficient with the decrease in the saturation. At the reference state ($C_r = 1$), the streaming potential coupling coefficient is equal to -5.79 , -3.97 , and -4.47 nV Pa^{-1} for the RFF2, BRAU2, and ESTA2 samples, respectively. In each case, measurements were compared with the laws established by Revil et al. (2007), based on the Brooks and Corey and the van Genuchten approaches, which predict a decrease in the streaming potential when the saturation decreases also (Eq. [15–16]). Models were fitted with the same Corey and van Genuchten exponents used above and predicted that the streaming potential coupling coefficient falls to zero at the irreducible water saturation. The same behavior was already observed by different researchers (e.g., Revil and Cerepi, 2004; Revil et al., 2007; Vinogradov and Jackson, 2011).

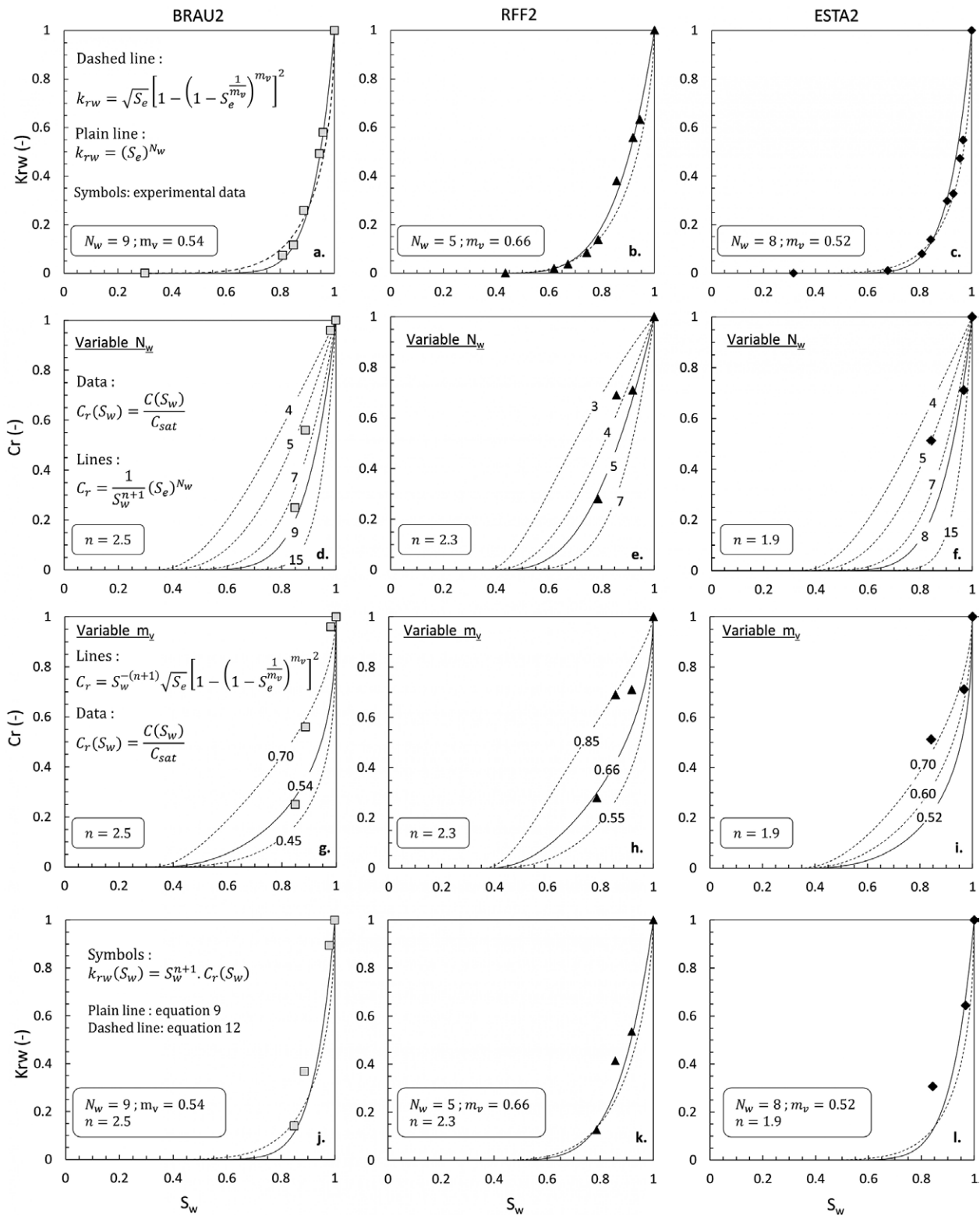


Fig. 4. Modeling of water drainage relative permeability on three carbonated rocks: (a–c) experimental data of water relative permeability for three limestone cores: BRAU2, RFF2, and ESTA2—data have been fitted with the Brooks and Corey model and the van Genuchten model; (d–f) relative streaming potential coupling coefficient for the three samples—at the reference state ($C_r = 1$), the streaming potential coupling coefficient is -3.97 , -5.79 , and -4.47 nV Pa $^{-1}$ for BRAU2 (gray squares), RFF2 (black triangles), and ESTA2 (black diamonds) samples, respectively, and the NaCl concentration of the electrolyte is 10 g L $^{-1}$ —these data are fitted (plain lines) with a model from Revil et al. (2007) (Eq. [15]) with the initial Corey exponent, while dashed lines represent Eq. [15] with variable N_w ; (g–i) relative streaming potential coupling coefficient fitted (plain lines) with a model from Revil et al. (2007) (Eq. [16]) with the initial van Genuchten exponent; and (j–l) water relative permeability of the three samples (same markers as above), calculated with the Revil et al. (2007) model (Eq. [14]). Data are compared with the Brooks and Corey model (plain lines) and van Genuchten models (dashed lines) with a quite good correlation.

Table 2. Calculated streaming potential coupling coefficient (C_{sat}) at a given NaCl concentration (C_f).

Sample	C_f	C_{sat}
	mol L ⁻¹	nV Pa ⁻¹
BRAU1	0.24	-5.00
BRAU2	0.17	-3.97
ESTA1	0.17	-7.20
ESTA2	0.17	-4.47
LAV1	0.17	-4.95
RFF1	0.17	-7.31
RFF2	0.17	-5.79
STE1	0.017	-51.7

Capillary Pressure

Capillary pressure curves were fitted with the van Genuchten exponent, m_v , (Fig. 9). We observe a good correlation between the model and capillary pressure data recorded from porous plate experiments. The entry pressure of water, P_e , which is a characteristic constant of the medium, has a value of 12, 33, and 16 kPa for the ESTA2, RFF2, and BRAU2 samples, respectively. In spite of the different experiments (steady-state flooding and porous plate), the van Genuchten exponent used to fit the capillary pressure model and the relative permeability model (above) described by van Genuchten (1980) is the same. This shows the consistency of the measurements in steady-state and porous-plate experiments.

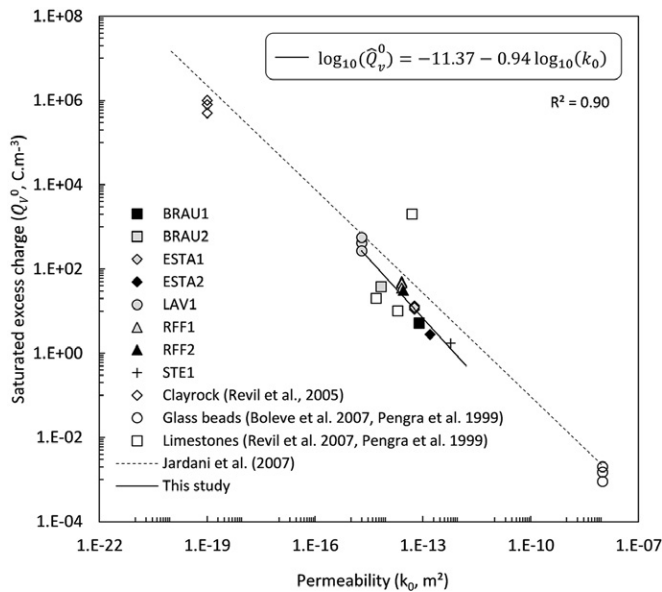


Fig. 5. Charge density at electrical conductivity $S_w = 1$ vs. the absolute water permeability for eight carbonate core samples studied: BRAU1, BRAU2, ESTA1, ESTA2, LAV1, RFF1, RFF2, and STE1. The relationship in carbonate rocks is also represented (solid line) as well as data from the literature: clayrocks (Revil et al., 2005), glass beads (Bolève et al., 2007; Pengra et al., 1999), and limestones (Revil et al., 2007; Pengra et al., 1999). The relationship in silica materials from Jardani et al. (2007) is also shown (dashed line).

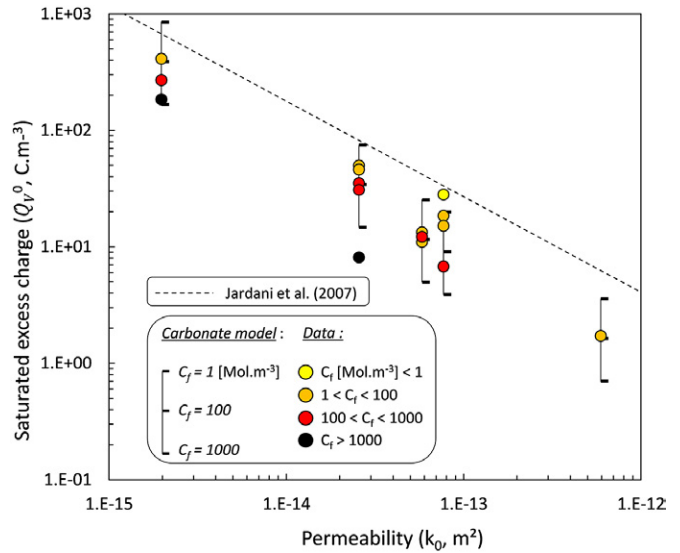


Fig. 6. Charge density at electrical conductivity $S_w = 1$ vs. the absolute water permeability for five carbonate core samples. Data were calculated for different brine salinities (C_f) and compared with the model of Guarracino and Jougnot (2018). We used the zeta potential trend of this study (Eq. [26]) and the tortuosity formula from Winsauer et al. (1952) in this model.

Zeta Potential

Figure 10 shows the zeta potential (calculated from the Eq. [18]) as a function of brine salinity for the samples investigated in this study. The magnitude of the zeta potential decreases with increasing salinity under atmospheric conditions, as observed in other studies that focused only on silica materials (e.g., Vinogradov et al., 2010). Vinogradov et al. (2010) found that the zeta potential reaches a constant value at salinity approximately above 0.4 mol L⁻¹. We don't have enough data to verify this point.

According to the studies of Jaafar et al. (2009) and Vinogradov et al. (2010) (Eq. [19]), the trend of the zeta potential in the carbonate samples investigated in this study is given by

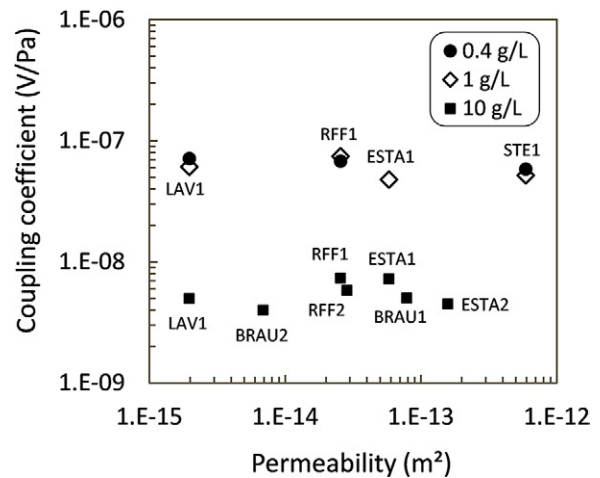


Fig. 7. Absolute value of the streaming potential coupling coefficient dependence on permeability. Measurements were performed with three different NaCl salinity rates: 0.4, 1.0, and 10.0 g L⁻¹.

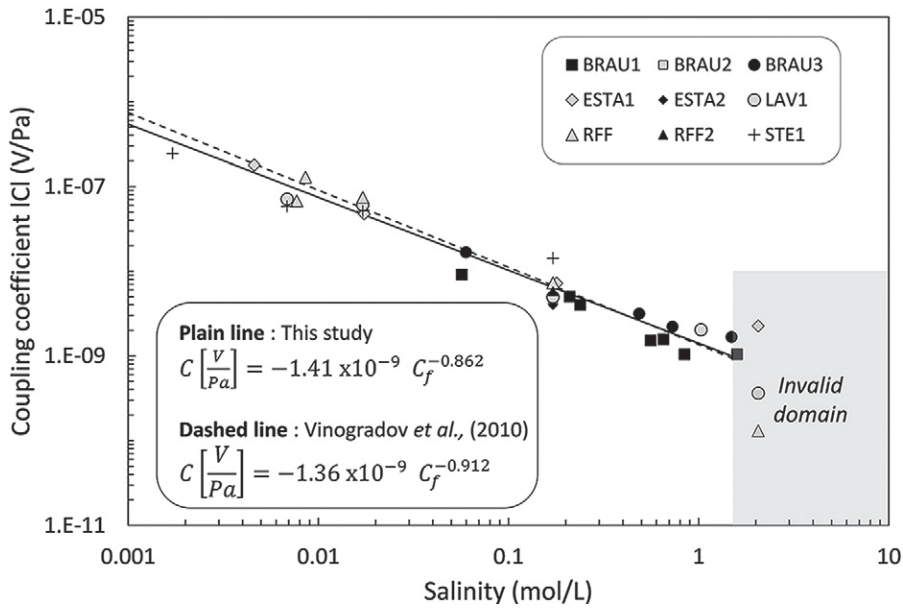


Fig. 8. Absolute value of the streaming potential coupling coefficient (C) as a function of salinity (C_f) in the range 0.002 to 1.5 mol L⁻¹ for nine sample of carbonate rocks: BRAU1, BRAU2, BRAU3, ESTA1, ESTA2, LAV1, RFF1, RFF2, and STE1. The fit of these data (Eq. [24]) (plain line, $R^2 = 0.94$) is quite the same as the fit found by Vinogradov et al. (2010) for silica materials (dashed line, $R^2 = 0.92$).

$$\zeta = 9.13 \log_{10} C_f - 6.97 \quad [26]$$

where C_f is the brine salinity (mol L⁻¹). The logarithmic equation has a theoretical argument in sandstones (Revil et al., 1999a) and seems applicable to limestone under atmospheric conditions without CO₂ partial pressure.

Discussion

Streaming Potential Coupling Coefficient Influence of Saturation

The relative streaming potential coefficient obtained from the data does not decrease monotonically with decreasing water saturation, as expected considering Eq. [5]. This effect is commonly accepted and has been shown in other studies (Revil and Cerepi, 2004; Revil et al., 2007; Jackson, 2010; Jougnot et al., 2012; Cerepi et al., 2017) when water is the wetting phase and the second phase (gas) is non-polar, and may be due to counterbalancing effects at partial water saturation between the conductivity, the permeability, and the excess charge density. Moreover, the excess charge density at partial saturation (Fig. 11a) was calculated from Eq. [5] using relative streaming potential coupling coefficient data and compared with Eq. [7] with a quite good correlation. This can confirm the non-monotonic trend between the relative streaming potential coefficient and the saturation.

Due to the complexity of measuring the streaming potential coupling coefficient during a drainage experiment, only a few data are available for the three samples investigated. Models imply a direct relationship between the relative streaming potential coupling coefficient and the saturation. This also includes petrophysical parameters, as the Corey exponent (N_w) (Brooks and Corey approach, Eq. [15]), the van Genuchten exponent (m_v) (van Genuchten approach, Eq. [16]), or the second Archie exponent (n) and therefore takes into account wettability effects. As

shown in Fig. 4d to 4i, the Corey and van Genuchten exponents have a huge influence on the models and imply the need to realize drainage experiments under rigorous conditions. The solid lines (Fig. 4d–4i) were fitted using Corey and van Genuchten exponents calculated from experimental relative permeability data and were used in the relative permeability model (see below). Although the Corey and van Genuchten exponents vary in magnitude at $N_w \pm 2$ and $m_v \pm 0.2$, respectively, the predicted and measured relative streaming potential coupling coefficients seem to follow the same trend ($R^2 = 0.83$ and $R^2 = 0.79$, respectively). Nevertheless, these models have some limits. When another nonaqueous or nonpolar phase (oil) is the wetting phase, the relative streaming potential coupling coefficient increases with decreasing water saturation (Jackson, 2010) and Eq. [15–16] cannot be applied.

Relative Permeability Model

The relative permeability model proposed by Revil et al. (2007) (Eq. [14]) was tested for the first time (to our knowledge) in this study with experimental data. It relies on the streaming potential measurements to predict water relative permeability, also using Archie's saturation exponent. Figure 4 shows the water relative permeability calculated from Eq. [14] (Fig. 4j–4l) and the water relative permeability curves fitted with experimental data, using both the Brooks and Corey (Eq. [9]) and the van Genuchten (Eq. [12]) models (Fig. 4a–4c). Measurements predicted from Eq. [14] and the experimental data are close (Fig. 11b, $R^2 = 0.95$), which confirms that this model gives a quite good approximation of the relative permeability when water is the wetting phase and the second phase is nonpolar.

Zeta Potential Dependence with Salinity

Jaafar et al. (2009) estimated that the diffuse layer collapses to zero when the salinity is >0.4 mol L⁻¹ in silica materials. Therefore, we only took into account zeta potential values <1 mol L⁻¹ of

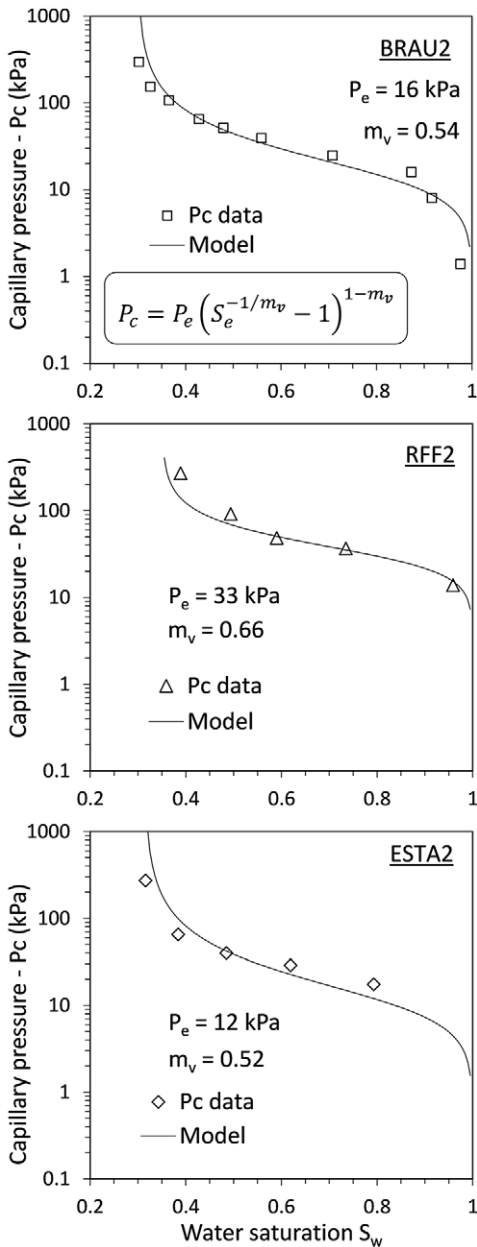


Fig. 9. Fit of the capillary pressure data (dashed lines) using the van Genuchten exponent m_v (van Genuchten, 1980) and capillary entry pressure of water (P_e). Note that the exponent m_v is the same as that used for the relative permeability model (0.52, 0.66, and 0.54 for the ESTA2, RFF2, and BRAU2 samples, respectively), showing the accuracy of the experimental measurements.

magnitude because the rock mineralogy does not seem to influence the streaming potential coupling coefficient values. A logarithmic relationship can connect the zeta potential and the salinity (Eq. [26]) (up to approximately 1 mol L^{-1}) (see Jaafar et al., 2009; Vinogradov et al., 2010), validating the model proposed by Revil et al. (1999a). The logarithmic trend seems applicable to limestone samples (Chen et al., 2014) under atmospheric conditions without CO_2 partial pressure. We expect that this result would be different under reservoir conditions, with CO_2 partial pressure, due to chemical reactions and catalysts as pressure and temperature. The

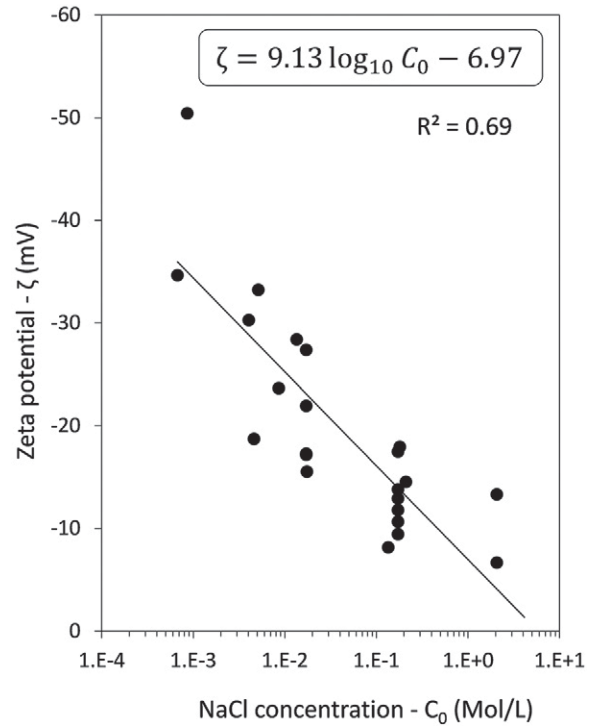


Fig. 10. Zeta potential vs. salinity, showing only our data (intact limestones, black circles), and the corresponding model (solid line) in the range 10^{-3} – 10^0 mol L^{-1} ($R^2 = 0.69$).

magnitude of the zeta potential at salinity $<1 \text{ mol L}^{-1}$ increases with decreasing salinity (Fig. 10), as observed in previous studies, but is lower than that observed in silica materials.

Excess Charge Density Dependence with Salinity

Guarracino and Jougnot (2018) argued that a higher salinity leads to a lower excess charge density in silica materials. They related \hat{Q}_v^0 from hydraulic (porosity, absolute permeability, tortuosity) and pore water (electrolyte concentration, Debye length, zeta potential) parameters. The only parameter affected by the rock mineralogy is the zeta potential, hence the interest in defining a specific law for the zeta potential in carbonates (Eq. [26]). Their model seems more robust than that of Jardani et al. (2007) because it takes into account the pore water chemistry. We can see the huge influence of the salinity on the saturated excess charge (Fig. 6), with a saturated excess charge approximately five times higher at a concentration of 1 mol m^{-3} than 1000 mol m^{-3} . The data are quite well correlated with the model of Guarracino and Jougnot (2018), which allows us at first sight to validate this model for carbonates with a monovalent electrolyte.

Conclusion

A core-scale experimental investigation was undertaken to investigate the relationships among the capillary pressure, the relative permeability, and the streaming potential coupling coefficient in carbonate rocks. We used pure NaCl brines and N_2 to perform

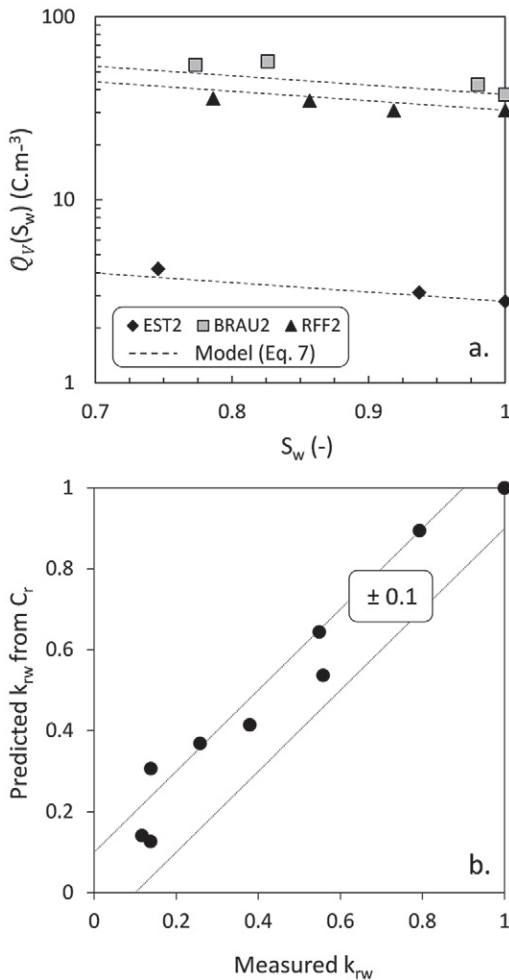


Fig. 11. (a) Excess charge density data (Q_V) at partial saturation (S_w) for three samples (EST2, BRAU2, and RFF2) compared with their respective models, and (b) predicted water relative permeability (k_{rw}) using Eq. [14] vs. experimental data ($R^2 = 0.95$).

measurements, using the steady-state flow method. The following conclusions were reached:

1. The magnitude of the streaming potential coupling coefficient decreases with increasing salinity as predicted by current models. The zeta potential in carbonate rocks can be related to salinity with a logarithmic law in the same way as for silica materials for salinity $<1 \text{ mol L}^{-1}$ under atmospheric conditions.
2. The volumetric charge density can be directly estimated from the quasi-static permeability at full saturation. Our values of volumetric charge density are in the same range as the empirical equation proposed by Jardani et al. (2007) on sandstones and are consistent with other values calculated on limestone samples (Pengra et al., 1999; Revil et al., 2007). The shift between the curves is partly attributed to the electrolyte salinity.
3. We were able to fit experimental data of the relative permeability, the relative streaming potential coupling coefficient, and the capillary pressure in a consistent way for carbonates using the van Genuchten approach and exactly the same value of the van Genuchten exponent.

4. The relative streaming potential coupling coefficient is strongly dependent on the saturation and decreases non-monotonically with it. The Brooks and Corey approach ($R^2 = 0.83$) provides a slightly better fit with experimental data than the van Genuchten approach ($R^2 = 0.79$).
5. The relative permeability model proposed by Revil et al. (2007), based on the relative streaming potential coupling coefficient, was tested under water-wet conditions and presented a quite good correlation with experimental measurements performed on three limestones ($R^2 = 0.95$).

Acknowledgments

This research has been supported by IFP Energies Nouvelles, Rueil-Malmaison, France. The contribution of A. Revil is supported by Université Savoie Mont-Blanc and Université Grenoble Alpes. Different experimental data and petrophysical analysis used in this study and shown in Fig. 1 to 11 are available to the public from the authors on request (aurelien.cherubini@ifpen.fr). We also thank the two referees for their very constructive comments and their time.

References

- Alroudhan, A., J. Vinogradov, and M.D. Jackson. 2016. Zeta potential of intact natural limestone: Impact of potential-determining ions Ca, Mg and SO_4 . *Colloids Surf. A* 493:83–98. doi:10.1016/j.colsurfa.2015.11.068
- Archie, G.E. 1942. The electrical resistivity log as an aid in determining some reservoir characteristics. *Trans. Am. Inst. Min. Metall. Eng.* 146:54–61.
- Bolève, A., A. Crespy, A. Revil, F. Janod, and J.L. Mattiuzzo. 2007. Streaming potentials of granular media: Influence of the Dukhin and Reynolds numbers. *J. Geophys. Res.* 112:B08204. doi:10.1029/2006JB004673
- Brooks, R.H., and A.T. Corey. 1964. Hydraulic properties of porous media. *Hydrol. Pap. 3*. Colorado State Univ., Fort Collins.
- Brooks, R.H., and A.T. Corey. 1966. Properties of porous media affecting fluid flow. *J. Irrig. Drain. Div. Am. Soc. Civ. Eng.* 92:61–90.
- Cerepi, A., A. Cherubini, B. Garcia, H. Deschamps, and A. Revil. 2017. Streaming potential coupling coefficient in unsaturated carbonate rocks. *Geophys. J. Int.* 210:291–302. doi:10.1093/gji/ggx162
- Chen, L., G. Zhang, L. Wang, W. Wu, and J. Ge. 2014. Zeta potential of limestone in a large range of salinity. *Colloids Surf. A* 450:1–8. doi:10.1016/j.colsurfa.2014.03.006
- Dukhin, S.S., and B.V. Derjaguin. 1974. *Electrokinetic phenomena*. Surface and Colloid Science 7. Wiley-Interscience, New York.
- Guarracino, L., and D. Jougnot. 2018. A physically based analytical model to describe effective excess charge for streaming potential generation in water saturated porous media. *J. Geophys. Res. Solid Earth* 123:52–65. doi:10.1002/2017JB014873
- Guichet, X., L. Jouniaux, and N. Catel. 2006. Modification of streaming potential by precipitation of calcite in a sand–water system: Laboratory measurements in the pH range from 4 to 12. *Geophys. J. Int.* 166:445–460. doi:10.1111/j.1365-246X.2006.02922.x
- Hunter, R.J. 1981. *Zeta potential in colloid science*. Academic Press, New York.
- Jaafar, M.Z., J. Vinogradov, and M.D. Jackson. 2009. Measurement of streaming potential coupling coefficient in sandstones saturated with high salinity NaCl brine. *Geophys. Res. Lett.* 36:L21306. doi:10.1029/2009GL040549
- Jackson, M.D. 2010. Multiphase electrokinetic coupling: Insights into the impact of fluid and charge distribution at the pore scale from a bundle of capillary tubes model. *J. Geophys. Res.* 115:B07206. doi:10.1029/2009JB007092
- Jardani, A., A. Revil, F. Santos, C. Fauchard, and J.P. Dupont. 2007. Detection of preferential infiltration pathways in sinkholes using joint inversion of self-potential and EM-34 conductivity data. *Geophys. Prospect.* 55:749–760. doi:10.1111/j.1365-2478.2007.00638.x

- Jougnot, D., N. Linde, E.B. Haarder, and M.C. Looms. 2015. Monitoring of saline tracer movement with vertically distributed self-potential measurements at the HOBE agricultural test site, Voulund, Denmark. *J. Hydrol.* 521:314–327. doi:10.1016/j.jhydrol.2014.11.041
- Jougnot, D., N. Linde, A. Revil, and C. Doussan. 2012. Derivation of soil-specific streaming potential electrical parameters from hydrodynamic characteristics of partially saturated soils. *Vadose Zone J.* 11(1). doi:10.2136/vzj2011.0086
- Kaszuba, J.P., D.R. Janecky, and M.G. Snow. 2003. Carbon dioxide reaction processes in a model brine aquifer at 200°C and 200 bars: Implications for geologic sequestration of carbon. *Appl. Geochem.* 18:1065–1080. doi:10.1016/S0883-2927(02)00239-1
- Krevor, S.C.M., R. Pini, L. Zuo, and S.M. Benson. 2012. Relative permeability and trapping of CO₂ and water in sandstone rocks at reservoir conditions. *Water Resour. Res.* 48:W02532. doi:10.1029/2011WR010859
- Lerouge, C., F. Claret, M.A. Denecke, G. Wille, G. Falkenberg, C. Ramboz, et al. 2010. Comparative EPMA and m-XRF methods for mapping micro-scale distribution of iodine in biocarbonates of the Callovian–Oxfordian clayey formation at Bure, eastern part of the Paris Basin. *Phys. Chem. Earth* 35:271–277. doi:10.1016/j.pce.2010.04.003
- Li, S., P. Leroy, F. Heberling, N. Devau, D. Jougnot, and C. Chiaberge. 2016. Influence of surface conductivity on the apparent zeta potential of calcite. *J. Colloid Interface Sci.* 468:262–275. doi:10.1016/j.jcis.2016.01.075
- Linde, N., D. Jougnot, A. Revil, S.K. Matthäi, T. Arora, D. Renard, and C. Doussan. 2007. Streaming current generation in two-phase flow conditions. *Geophys. Res. Lett.* 34:L03306. doi:10.1029/2006GL028878
- Mboh, C.M., J.A. Huisman, E. Zimmermann, and H. Vereecken. 2012. Coupled hydrogeophysical inversion of streaming potential signals for unsaturated soil hydraulic properties. *Vadose Zone J.* 11(2). doi:10.2136/vzj2011.0115
- Overbeek, J.T.G. 1952. Electrochemistry of the electrical double layer. In: H.R. Kruyt, editor, *Colloids science*. Vol. 1. Irreversible systems. Elsevier, Amsterdam. p. 115–193.
- Pengra, D.B., S. Xi Li, and P. Wong. 1999. Determination of rock properties by low-frequency AC electrokinetics. *J. Geophys. Res.* 104(B12):29485–29508. doi:10.1029/1999JB900277
- Pride, S., and F.D. Morgan. 1991. Electrokinetic dissipation induced by seismic waves. *Geophysics* 56:914–925. doi:10.1190/1.1443125
- Revil, A., and A. Cerepi. 2004. Streaming potentials in two-phase flow conditions. *Geophys. Res. Lett.* 31:L11605. doi:10.1029/2004GL020140
- Revil, A., P. Leroy, and K. Titov. 2005. Characterization of transport properties of argillaceous sediments: Application to the Callovo-Oxfordian argillite. *J. Geophys. Res.* 110:B06202. doi:10.1029/2004JB003442
- Revil, A., N. Linde, A. Cerepi, D. Jougnot, S. Matthäi, and S. Finsterle. 2007. Electrokinetic coupling in unsaturated porous media. *J. Colloid Interface Sci.* 313:315–327.
- Revil, A., and H. Mahardika. 2013. Coupled hydromechanical and electromagnetic disturbances in unsaturated porous materials. *Water Resour. Res.* 49. doi:10.1002/wrcr.20092
- Revil, A., P.A. Pezard, and P.W.J. Glover. 1999a. Streaming potential in porous media: 1. Theory of the zeta potential. *J. Geophys. Res.* 104(B9):20021–20031. doi:10.1029/1999JB900089
- Revil, A., H. Schwaeger, L.M. Cathles, and P.D. Manhardt. 1999b. Streaming potential in porous media: 2. Theory and application to geothermal systems. *J. Geophys. Res.* 104(B9):20033–20048.
- Saunders, J.H., M.D. Jackson, and C.C. Pain. 2008. Fluid flow monitoring in oil fields using downhole measurements of electrokinetic potential. *Geophysics* 73(5):E165–E180. doi:10.1190/1.2959139
- Sill, W.R. 1983. Self-potential modeling from primary flows. *Geophysics* 48:76–86. doi:10.1190/1.1441409
- Stern, O. 1924. Theory of the electrical double layer. *Electrochemistry* 30:508–516.
- Thony, J.L., P. Morat, G. Vachaud, and J.L. Le Mouél. 1997. Field characterization of the relationship between electrical potential gradients and soils water flux. *C.R. Acad. Sci., Ser. Ila* 325:317–325.
- van Genuchten, M.Th. 1980. A closed form equation for predicting the hydraulic conductivity of unsaturated soils. *Soil Sci. Soc. Am. J.* 44:892–898. doi:10.2136/sssaj1980.03615995004400050002x
- Vinogradov, J., M.Z. Jaafar, and M.D. Jackson. 2010. Measurement of streaming potential coupling coefficient in sandstones saturated with natural and artificial brines at high salinity. *J. Geophys. Res.* 115:B12204. doi:10.1029/2010JB007593
- Vinogradov, J., and M.D. Jackson. 2011. Multiphase streaming potential in sandstones saturated with gas/brine and oil/brine during drainage and imbibition. *Geophys. Res. Lett.* 38:L01301. doi:10.1029/2010GL045726
- Winsauer, W.O., H. Shearin, Jr., P. Masson, and M. Williams. 1952. Resistivity of brine-saturated sands in relation to pore geometry. *AAPG Bull.* 36:253–277.
- Wolthers, M., L. Charlet, and P. Van Cappellen. 2008. The surface chemistry of divalent metal carbonate minerals: A critical assessment of surface charge and potential data using the charge distribution multi-site ion complexation model. *Am. J. Sci.* 308:905–941. doi:10.2475/08.2008.02
- Wolthers, M., D. Di Tommaso, Z. Du, and N.H. de Leeuw. 2012. Calcite surface structure and reactivity: Molecular dynamics simulations and macroscopic surface modelling of the calcite–water interface. *Phys. Chem. Chem. Phys.* 14:15145–15157. doi:10.1039/c2cp42290e
- Xu, T.F., J.A. Apps, and K. Pruess. 2003. Reactive geochemical transport simulation to study mineral trapping for CO₂ disposal in deep arenaceous formations. *J. Geophys. Res. Solid Earth* 108:2071. doi:10.1029/2002JB001979
- Zullig, J.J., and J.W. Morse. 1988. Interaction of organic acids with carbonate mineral surfaces in seawater and related solutions: I. Fatty acid adsorption. *Geochim. Cosmochim. Acta* 52:1667–1678. doi:10.1016/0016-7037(88)90235-9